Electronic pseudocharge model for the Cu(111) longitudinal-surface-phonon anomaly observed by helium-atom scattering

C. Kaden,* P. Ruggerone, J. P. Toennies, G. Zhang,† and G. Benedek‡
Max-Planck-Institut für Strömungsforschung, Bunsenstrasse 10, D-3400 Göttingen, Germany
(Received 9 December 1991)

The phonon-dispersion curves of the Cu(111) surface have been calculated in the framework of an electronic multipole model. The electronic pseudocharges are located at the midpoints between nearest-neighbor ions of the lattice and are expanded in terms of their dipole and quadrupole deformabilities. The anomalous longitudinal resonance observed by helium-atom scattering (HAS) is accounted for by increasing the dipolar and quadrupolar bulk deformabilites at the surface. Moreover the model explains in a straightforward way the apparent contradiction between force constants obtained from a fit of the HAS data and of similar dispersion curves measured by electron scattering. Thus the enhanced inelastic HAS intensity of the longitudinal resonance, which previously required extreme force-constant adjustments, is instead attributed to an additional contribution from the inelastic interaction of the He atoms with the dipolar and quadrupolar modulations of the surface electron density.

I. INTRODUCTION

Structural changes such as relaxation and reconstruction[1] indicate that at the surface of a crystal the forces between atoms are different than those in the bulk. These phenomena illustrate how the reduction in dimensionality at surfaces provide a sensitive test of physical models of a solid. More direct information on the forces at surfaces is now becoming available from measurements of surface-phonon-dispersion curves by the two complementary techniques of inelastic electron scattering[2] (EELS) and helium-atom scattering[1,3] (HAS). It is important for the later discussion to recall that the interaction of electrons and He atoms with the surface atoms is fundamentally different. In EELS as in low-energy electron diffraction (LEED) the high-energy (100–200-eV) electrons penetrate several layers into the crystal where they interact mostly with the inner shells of the ions, whereas the low-energy ($\approx$20-meV) helium atoms are scattered from the outer electrons with a density of only about 10^{-3} Å^{-2} at distances of about 3 Å above the first layer of atoms.

One of the most surprising observations made already in the first He phonon studies of metal surfaces was the discovery of an anomalous dispersion curve attributed to a longitudinal resonance in the closed-packed (111) surfaces of the noble metals Cu, Ag, and Au.[4–6] For Ag and Au, Bortolani, Santoro, and co-workers explained the appearance of this mode by assuming a large softening of the first-layer longitudinal force constant of 30% and 70%, respectively.[7–9] This strong reduction was attributed to electron spillout which weakens the *sp-d* hybridization in the surface layer. The phenomenon is nevertheless unexpected since these surfaces, with the exception of Au(111), do not show any significant relaxation nor reconstruction. The HAS-measured surface phonon dispersion curves for Cu(111) along the $\bar{\Gamma}$-$\bar{M}$ direction have recently been confirmed by EELS experiments, reported by Mohamed, Kesmodel, Hall, and Mills.[10] In addition to the longitudinal resonance, they were able to detect a longitudinal-gap surface mode, designated S_2, with an energy of 26 meV at the zone boundary. These data were analyzed with a single radial force-constant model for the bulk and could be fitted with only a 15% softening of the longitudinal intraplanar force constant in the first layer. Such force-constant models, however, appear to be entirely inadequate to reproduce HAS intensities associated with the longitudinal resonance. A recent unpublished analysis by Bortolani, Franchini, and Santoro[11] of the new He data for the Cu(111) surface presented in Sec. II shows that the simultaneous fit of surface phonon frequencies and HAS intensities requires a 67% *softening* of the longitudinal (intraplanar) force constant and, in addition, a 60% *stiffening* of the force constant between the first two layers. These large, rather unphysical perturbations, while compensating each other to give still a good fit of the dispersion curves, cooperate in giving the polarization vectors a sufficiently large vertical component to account for the large intensity of the longitudinal mode with respect to the Rayleigh mode observed along both symmetry directions. This apparent contradiction between force constants from EELS data, on the one hand, and from He-atom scattering, on the other hand, which has been referred to as the "Bortolani-Mills paradox,"[12] calls for a critical reexamination of the dynamical interaction of the atoms with a metal surface.[13]

In the theory used by Bortolani and Santoro,[7,17–19] this interaction is described by a summation of additive two-body potentials between the impinging He atom and the surface atoms of the top layer. Celli, Eichenauer, Kaufhold, and Toennies[20] have demonstrated that with a realistic two-body potential, this theory with only one adjustable potential parameter is able to explain all the scattering observations for He scattering from LiF(001), including diffraction intensities, selective adsorption resonances, and the Rayleigh wave inelastic intensities, very successfully. For the metal surfaces Cu(111) and

Ag(111), a similar additive potential model was also able to predict the *Rayleigh* inelastic intensities over the entire range of phonon wave vectors.[21] No attempt was, however, made to fit the *longitudinal* resonance. In this work and in Ref. 19, the predicted diffraction intensities were larger than actually observed. This was accounted for by including the Smoluchowski electron smoothing[22] of the surface potential corrugation.

If the surface electrons affect the diffraction, it would appear that they might also affect the inelastic coupling of the He atoms with the surface phonons.[23] To account for this interaction, we need to understand how the electrons of a metal couple to the lattice vibrations, especially at the surface. In addition, we have to estimate the coupling of the He atoms to the vibrations via an interaction with the delocalized conduction electrons as well as with the localized valence electrons bound to the ion cores. There has been considerable progress in the first-principles calculation of surface-phonon-dispersion curves for aluminum surfaces in the local-density approximation of density-functional theory[24,25] and for the more complicated metals such as Au(110) (Ref. 26) and recently even for Cu(111) (Ref. 27). However, these methods do not provide information on the electronic distortions accompanying the lattice vibrations and cannot therefore be used to model the dynamics of He scattering.

To deal with this problem, we have further developed a semiempirical lattice-dynamical model of metals based on the idea that the ions couple not only with each other directly but also indirectly via an *adiabatic* coupling to the electrons. The electrons are thus introduced as pseudoparticles with negligible mass (ghosts) but are endowed with deformabilities with well-defined symmetries matched to the motions of the surrounding ion cores. The idea behind this model is similar in spirit to the very successful shell model of insulators[28,29] or the bond-charge model for semiconductors.[30] Its application to bulk materials was first suggested as early as 1971 by Hanke and Bilz.[31,32] Similar models have been developed and applied to the calculation of bulk phonons in metals by Wakabayashi,[33] Allen,[34] and recently by Li and Goddard.[35] The model was first applied to the calculation of surface-phonon-dispersion curves of the noble metals by Jayanthi, Bilz, Kress, and Benedek.[36] With a physically justified adjustment of the surface force constants, it was possible to explain the anomalous longitudinal mode in Cu(111) and Ag(111), but only partially in Au(111). In this early study the electron pseudocharges were located at points of high symmetry. This had the advantage of introducing the least number of pseudocharges, but the disadvantage that, in fact, they were located in positions with the lowest electron density and, moreover, that considerable adjustments were needed to satisfy the boundary conditions at the surface. Here we have considered a more refined choice of the pseudocharge expansion points by placing them at the midpoints between nearest-neighbor ions. Since these are at the expected saddle points of the electron density[37] for this particular choice, we may speak of bond pseudocharges. The deviations from the Cauchy relations are accounted for by including the quadrupolar deformation to mimic many-body effects. Thus this model gives not only a rather accurate mapping of the conduction-electron charge distribution but also its dynamic fluctuations within the unit cell as indicated by the very good fit of the bulk dispersion curves. With only five parameters, the fitted surface dispersion curves for a slab of 33 atomic layers reproduce very well the experimental dispersion of the Rayleigh waves, as well as that of the longitudinal resonance and of the gap mode.

The present choice of the expansion points is also quite convenient for modeling the dynamics of the (111) surface, because all the pseudocharges are now located in the surface plane and do not have to be displaced as in the earlier model[36] in order to recover equilibrium. The new pseudocharge model also offers a suitable framework for estimating the inelastic-scattering amplitudes, for either He atoms or electrons, through the oscillations of electronic coordinates. As an example, we report the surface-phonon densities projected onto the electronic degrees of freedom. They contain information on the frequency-dependent mean-square dipolar and quadrupolar oscillations of the conduction electrons at the surface during the atomic motion. Such electron density oscillations may be converted into modulations of the particle-surface potential and hence into scattering amplitudes via, e.g., the Nørskov criterion.[38] In this way it has been possible to calculate the time-of-flight spectra and compare the model directly with experiment. We obtain the important result that the comparatively large scattering amplitude of the longitudinal resonance approaching the zone boundary comes essentially from the quadrupolar deformation of the surface charge, and to a minor extent from the dipolar part. On the contrary, the dipolar deformation at the first layer contributes strongly to the density of states of a flat branch at about 26 meV. This may be related to the large intensity of this mode in EELS experiments.[10] The previous interpretation of the EELS mode[10] attributed it entirely to ion-core displacements in the second layer. Thus, the present lattice-dynamical model provides a more realistic description of the surface phonons and their coupling to the probe particles than either of the force-constant models used by Bortolani and co-workers and by Mills and co-workers.

The paper starts with a presentation of new He-scattering data for the phonons on the Cu(111) surface. The electronic pseudocharge model is described and discussed next. In Sec. IV the model is applied to predicting the bulk-phonon-dispersion curves of Cu. The calculations of surface-phonon-dispersion curves for Cu(111) are then presented and compared with the experimental results. The role of pseudocharges in the dynamic corrugation of the surface is illustrated through the calculation of the surface-projected phonon densities of states. Finally, the He-scattering time-of-flight (TOF) spectra are simulated by including the interactions with the pseudocharges. The paper closes with a discussion of other evidence in support of the model used.

II. EXPERIMENTAL RESULTS

In view of the controversial interpretation of the earlier HAS surface-phonon data, new experiments were carried

out. The experimental techniques[1,39] and the methods of crystal preparation and characterization are essentially the same as used in the earlier work.[5] The improvements in the new data over the earlier work result from the cumulative effect of a large number of, in themselves, minor technical modifications made since the first set of measurements was reported in 1985.

Figures 1 and 2 show some typical time-of-flight spectra taken for the two symmetry directions. In all cases there is clear evidence for two well-resolved inelastic peaks, of which the one with the greatest energy transfer is attributed to the longitudinal anomaly.[40] Figure 3 compares the new surface-phonon-dispersion curves from the HAS data with the EELS data, which is only available for the ⟨112⟩ direction. It is seen that the two sets of data are in reasonable agreement not only for the Rayleigh mode but also for the anomalous longitudinal mode in the ⟨112⟩ direction. In addition, the EELS data contain a few points which pin down the location of the gap mode S_2 and provide some evidence for a surface mode just below the uppermost bulk band edge. For comparison the band edges and surface modes of a calculation based on a single constant fitted to the bulk are also shown.

Whereas the two sets of experimental dispersion curves appear to be in reasonable agreement, their interpretation

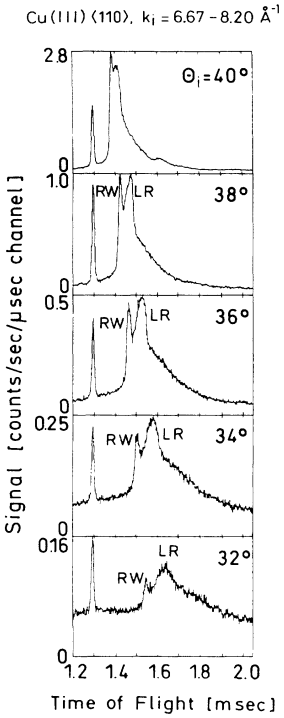

FIG. 1. Time-of-flight spectra measured for the scattering of He atoms with incident energies in the range between $E_i = 23.2$ and 35.0 meV ($k_i = 6.67$–8.20 Å^{-1}) from Cu(111) along the ⟨110⟩ azimuth for a surface temperature of $T_s = 160$ K. The first peak with the smallest energy transfer is attributed to the Rayleigh mode (RW), and the second peak, which is more intense at angles removed from the specular, is atrributed to the longitudinal resonance (LR).

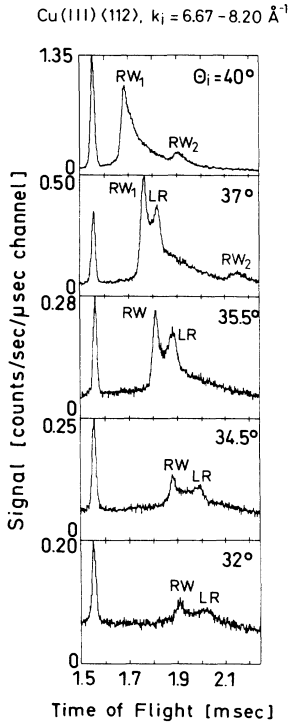

FIG. 2. Time-of-flight spectra measured for the scattering of He atoms with incident energies in the range between $E_i = 23.3$ and 35.0 meV ($k_i = 6.67$–8.20 Å^{-1}) from Cu(111) along the ⟨112⟩ azimuth for a surface temperature of $T_s = 160$ K. The second peak designated with an RW_2 in the spectra at $\Theta_i = 40°$ and 37° is due to an interaction with another higher-energy part of the Rayleigh dispersion curve.

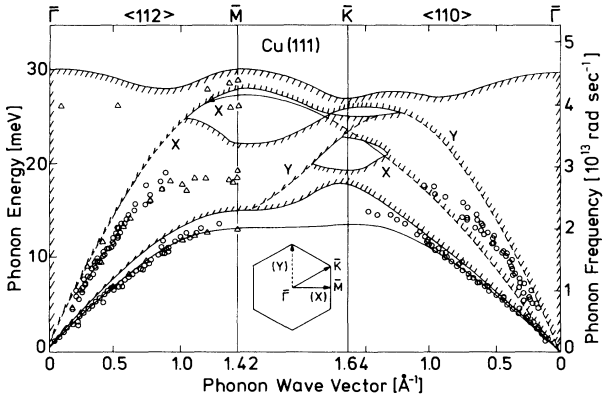

FIG. 3. Comparison of the present HAS experimental dispersion curves (○) for Cu(111) for both symmetry direction with the EELS data (△) reported in Ref. 10. The surface modes and bulk band boundaries are from a calculation based on a single bulk force constant fitted to bulk phonons (Ref. 41). The X and Y designations refer to the polarizations of the corresponding modes as identified in the reduced zone diagram in the inset. The surface temperature for the HAS data is 160 K and for the EELS data, 300 K.

leads to vastly different results for the force-constant changes at the surface, as mentioned in the Introduction. Here it is important to realize that the interpretation of phonon-dispersion curves is only unique if the polarization of the modes is purely accounted for[42] by also fitting the inelastic intensities. Table I summarizes the surface force constants determined by the different groups. With regard to the bulk force constants, the only difference between the data analysis of the EELS and HAS data arises from the number of terms in the Born–von Karman fitting procedure. Bortolani, Franchini, and Santoro went to great effort to fit not only the bulk-dispersion curves to better than 2% but also the elastic constants. To satisfy the breakdown of the Cauchy relations, they had to include three-body angle-bending forces described by the force constant δ_n^b.[43] Altogether, 14 force constants were determined, of which only the larger ones are shown in Table I. As expected, the largest force constant, the nearest-neighbor radial force constant β_1^b, is nearly the same as the single force constant used by Hall *et al.*[10] At the surface, however, the group of Hall *et al.* find it necessary to reduce the interplanar force constant $\beta_{\parallel}^s$ by only 15% in order to fit both the longitudinal mode[10] and the S_2 gap mode. The fit of the S_2 gap mode is found to be especially sensitive to $\beta_{\parallel}^s$. A softening by 30%, which is equivalent to the softening obtained by Jayanthi *et al.* with the pseudocharge model,[36] is definitely not compatible with the energy of the S_2 mode. Recent calculations in our laboratory similar to those reported by Hall *et al.*[10] lead to somewhat different results.[44]

In their fit of the surface-phonon data Santoro *et al.* find, however, that much larger force-constant changes are needed. The problem is not so much to fit the dispersion curves but rather the relative intensity of the longitudinal-mode peak with respect to the Rayleigh mode. This is illustrated for a typical time-of-flight spectrum shown in Fig. 4.[11] The dashed line shows the simulated time-of-flight spectrum calculated with the one force-constant model of Hall *et al.* with a 15% softening of the intraplanar (longitudinal) force constant in the surface plane. Similar differences between the predicted and measured time-of-flight spectra were found for all the other time-of-flight spectra for both symmetry directions.[11] The solid-line results are from a calculation based on a 67% softening of $\beta_{\parallel}^s$ and a 60% stiffening of $\beta_{\perp}^s$. Obviously, the latter calculation provides a better fit

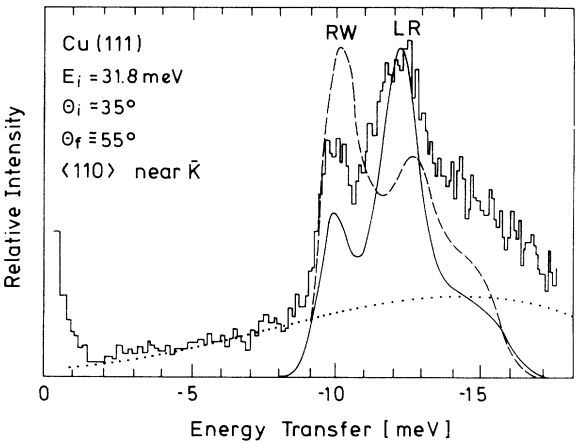

FIG. 4. Comparison of two different computer simulations of the time-of-flight spectra with the HAS experiment measured for $E_i = 31.8$ meV ($k_i = 7.8$ Å^{-1}) at an incident scattering angle of $\Theta_i = 35°$ ($T_s = 160$ K) assuming only single phonon interactions. RW and LR mark the peaks attributed to the Rayleigh mode and the longitudinal resonance, respectively. The calculated spectrum for a one-force-constant model with a 15% softening in the surface intraplanar force constant (dashed line) is not able to explain the relative experimental peak intensities. A calculation with a 67% softening of the intraplanar force constant and a 60% stiffening of the force consatnt between the outer layers (solid line) provides a much better fit of the peak positions and relative intensities. The dotted line shows a calclation of the energy-loss distribution for multiphonon excitation without a one-phonon contribution.

TABLE I. Comparison of best-fit surface force constants with bulk force constants (all values in N/m) determined from an analysis of EELS and HAS data of surface-dispersion curves for Cu(111).

Data fitted	Bulk force constants[a]	Surface force constants[b]	Reference
EELS	$\beta_1^b = 27.0$	$\beta_{\parallel}^s = 0.85\beta^b$ $\beta_{\perp}^s = 1.0\beta^b$	Hall *et al.* (Ref. 10)
HAS	$A_{\text{eff}} = 30.3$	$\beta_{\parallel}^s = 0.70 A_{\text{eff}}$[c] $\beta_{\perp}^s = 1.0 A_{\text{eff}}$[c]	Jayanthi *et al.* (Ref. 36)
HAS	$\alpha_1^b = -0.20$, $\beta_1^b = -31.34$, $\delta_1^b = -0.49$, $\alpha_2^b = -0.32$, $\beta_2^b = 0.11$, $\delta_2^b = -0.47$, etc.	$\beta_{\parallel}^s = 0.33\beta_1^b$ $\beta_{\perp}^s = 1.59\beta_1^b$	Bortolani *et al.* (Ref. 11)
HAS, EELS	$A_{\text{eff}} = 35.0$	$\beta_{\parallel}^s \equiv A_{\text{eff}}^s = 0.70 A_{\text{eff}}$ $\beta_{\perp}^s = 1.0 A_{\text{eff}}$	Present work

[a]The indices 1,2 refer to the first and second nearest neighbors.

[b]$\beta_{\parallel}$ denotes the intraplanar force constant (within the first layer), $\beta_{\perp}$ the interplanar force constant (between the first and second layers).

[c]This value was not reported by Jayanthi *et al.* (Ref. 36) but was established as an effective value by Hall *et al.* (Ref. 10) by fitting the gap mode calculated in Ref. 36.

of both the peak positions and the relative intensities of the HAS time-of-flight spectra.

A further comparison between the two previously outlined force-constant approaches is furnished by the surface densities of states, given by

$$\rho_{\alpha\alpha}(\mathbf{Q},E)=\sum_j |u_\alpha(1|\mathbf{Q},j)|^2\delta(E-\hbar\omega(\mathbf{Q},j)) , \quad (1)$$

where $u_\alpha(1|\mathbf{Q},j)$ is the ionic displacement vector of the atom in the surface layer (1) along the α direction. They are compared in Fig. 5 (Ref. 45), where the dashed lines are calculated with the surface force constants proposed by Mohamed *et al.*[10] and the solid lines are obtained by Bortolani, Franchini, and Santoro.[11] The latter calculation, as already pointed out in the above discussion of the TOF simulations, shows a very good agreement with the experimental data. It is worthwhile noting the behavior of the peak associated with the longitudinal resonance (LR) in the shear-vertical polarized phonon density of states (DOS), which is denoted by ρ_{zz}. At $\bar{M}/2$ [Fig. 5(a)] its intensity is large and only slightly lower than the intensity of the Rayleigh-wave (RW) peak. At the zone boundary [Fig. 5(b)], the ρ_{zz} DOS of the LR peak increases and exceeds that of the RW peak in good agreement with the experimental TOF. This is indicative of a hybridization of the two modes accompanied by a changeover in polarization. However, this calculation has the shortcoming that it also predicts an additional surface mode at about 31 meV which is shifted upwards out of the maximum of the bulk bands. The results of Mohamed *et al.* do not exhibit this feature and thus it probably is an artifact resulting from the unphysically large changes in the surface force constants. From an examination of Fig. 5, it is evident that the one force-constant calculations of Mohamed *et al.* do not accurately describe the Rayleigh-wave and longitudinal-resonance peak positions and their relative intensities. For example, at the position of the longitudinal resonance, there is no pronounced peak in the shear-vertical density of states ρ_{zz} which is needed to explain the HAS-TOF spectra. Thus, Fig. 5 clearly indicates that, in fact, neither of the force-constant parametrizations can explain all the data in a satisfactory way.

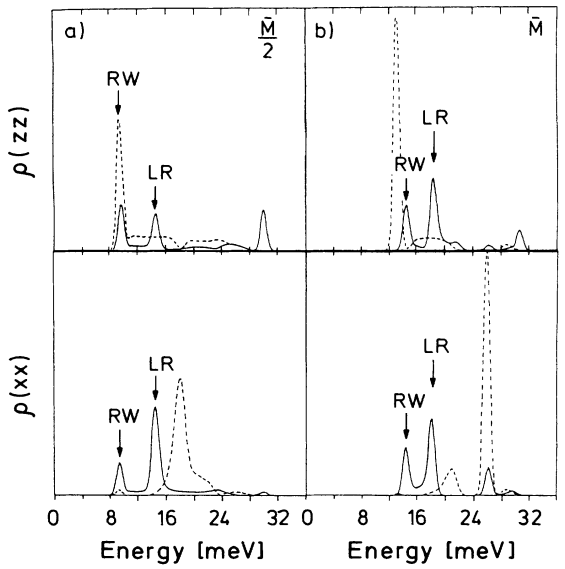

FIG. 5. Calculated relative phonon densities of states at (a) half-way between $\bar{\Gamma}$ and $\bar{M}$ ($\bar{M}/2$) and (b) at $\bar{M}$ (Ref. 45). The continuous lines are calculated with the best-fit force constants of Bortolani, Franchini, and Santoro (Ref. 11), the dashed lines are obtained with the force constants proposed by Mohamed *et al.* (Ref. 10). The densities of states are normalized to 1.

Recent work indicates that multiphonon processes also cannot explain the discrepancy. The results of a multiphonon calculation of HAS inelastic intensities based on the formula of Brako and Newns,[46] which has recently been successfully tested by a more accurate calculation,[16] yield the dotted line in Fig. 4. Obviously, multiphonon excitation also cannot explain the observed differences.[47]

III. THE PSEUDOCHARGE MULTIPOLE MODEL

As opposed to the two Born–von Kármán force-constant schemes compared above, the lattice-dynamical model used in the present paper accounts explicitly for the electronic degrees of freedom. The electron density within each unit cell is expanded in multipole components around symmetry points, and the expansion coefficients are treated as time-dependent dynamical variables similar to the ion displacements with which they are coupled. The choice of symmetry points is justified by the best convergence with regard to the number of electronic degrees of freedom. The coupling of the electronic with the ionic coordinates is treated in the adiabatic approximation. In this approach the coupling force constants may be either adjustable parameter or can, in principle, be obtained from a density-functional calculation. The phenomenological version of the electronic multipole model, used here, has the advantage over the Born–von Kármán force-constant model in that both bulk- and surface-dispersion curves as well as the elastic constants are nicely reproduced with a comparatively smaller number of parameters. Four of the five parameters can be understood in terms of a dynamic mixing of well-defined electronic band states, with dipole polarizabilities associated with p states and quadrupole polarizabilities associated with d states. Of course, higher-order terms can also be added if necessary.

The basic model used here can be derived from density-functional theory[48] by considering the total energy of the system as a sum of the total energies of the ions E_i and of the electrons E_e:

$$E=E_i+E_e[n] . \quad (2)$$

The energy of the electrons is a unique functional of the electron density $n(r)$,

$$E_e[n]=F[n]+\int w(r)n(r)d^3r , \quad (3)$$

where the functional F includes the electron-electron potential, as well as the kinetic and exchange-correlation energies, and $w(r)$ is the external potential acting on the electron system. In our case, $w(r)$ is the potential of the

ions at their instantaneous positions.

We perform a partition of the electron density into contributions associated with each unit cell:

$$n(\mathbf{r})=\sum_{l} n_l(\mathbf{r}) , \tag{4}$$

where l labels the unit cells of the lattice. Each partial density n_l is then mapped within the unit cell over a set of special points r_{lj}, e.g., a set of equivalent symmetry points, by performing the multipole expansion

$$n_l(\mathbf{r})=\sum_{j,\Gamma k} c_{\Gamma k}(lj) Y_{\Gamma k}(\mathbf{r}-\mathbf{r}_{lj}) . \tag{5}$$

Each basis function $Y_{\Gamma k}$ is the product of an appropriate radial function $R_{\Gamma k}$ and some harmonic function, which transforms according to the kth component of the Γth irreducible representation of the point group at $\mathbf{r}_{lj}$.[49] Spherical harmonics—more precisely, their combinations transforming as Γ—appear to be a particularly good choice. The set of special points should be chosen to have a rapid convergence with the smallest number of multipoles. On the other hand, a larger number of equivalent low-symmetry points will provide a more realistic mapping of the electronic density than a smaller number of high-symmetry points. The electrons in these points will be referred to as pseudocharges.

The expansion coefficients $c_{\Gamma k}(lj)$ in the multipolar representation act in the lattice dynamics as time-dependent variables dynamically coupled to the ion coordinates. They are the components of a pseudovector $\mathbf{c}(lj)$ which transform as the respective irreducible representations Γ. Such multipolar components will follow the ionic motion performing distortions $\Delta c_{\Gamma k}$ around the equilibrium values $c_{0,\Gamma k}(lj)$. The latter correspond to the ground-state density $n_0(\mathbf{r})$, which minimizes the total crystal energy when the ions are at their equilibrium position. Thus, in the multipole representation the electronic ground state may be defined by the conditions

$$\partial E/\partial c_{\Gamma k}(lj)=0 \quad (\text{for all } \Gamma,k,j) . \tag{6}$$

The total energy is then expanded in a Taylor series for a given equilibrium structure ($\{r_0\}$) not only with respect to the ionic displacements u_l but also with respect to the electronic multipole distortions $\Delta c(lj)$:

$$E=E_0+\tfrac{1}{2}\sum_{\substack{l\alpha\\ l'\beta}}\Phi_{\alpha\beta}(ll')u_\alpha(l)u_\beta(l')+\tfrac{1}{2}\sum_{\Gamma}\sum_{\substack{ljk\\ l'\alpha}}[\Phi_{\alpha k}(\Gamma;l',lj)u_\alpha(l')\Delta c_{\Gamma k}(lj)+\Phi_{k\alpha}(\Gamma;lj,l')u_\alpha(l')\Delta c_{\Gamma k}(lj)]$$
$$+\tfrac{1}{2}\sum_{\Gamma\Gamma'}\sum_{\substack{ljk\\ l'k'k'}}\Phi_{kk'}(\Gamma,\Gamma';lj,l'j')\Delta c_{\Gamma k}(lj)\Delta c_{\Gamma' k'}(l'j') , \tag{7}$$

where E_0 is set equal to zero and $\Phi_{\alpha\beta}$, $\Phi_{\alpha k}$, and $\Phi_{kk'}$ are the harmonic force constants for the ion-ion, ion-multipole, and the multipole-multipole interactions, respectively. They are defined by

$$\Phi_{\alpha\beta}(ll')=\frac{\partial^2 E}{\partial u_\alpha(l)\partial u_\beta(l')} , \tag{8a}$$

$$\Phi_{\alpha k}(\Gamma;l',lj)=\frac{\partial^2 E}{\partial u_\alpha(l')\partial c_{\Gamma k}(lj)}=\int d^3r\frac{\partial}{\partial u_\alpha(l')}\frac{\delta E}{\delta n(\mathbf{r})}Y_{\Gamma k}[\mathbf{r}-\mathbf{r}(lj)] , \tag{8b}$$

$$\Phi_{kk'}(\Gamma\Gamma';ljl'j')=\frac{\partial^2 E}{\partial c_{\Gamma k}(lj)\partial c_{\Gamma' k'}(l'j')}$$
$$=\int\int d^3r\, d^3r'\frac{\delta^2 E}{\delta n(\mathbf{r})\delta n(\mathbf{r}')}Y_{\Gamma k}[\mathbf{r}-\mathbf{r}(lj)]Y_{\Gamma' k'}[\mathbf{r}'-\mathbf{r}(l'j')] . \tag{8c}$$

In addition, we note that, in principle, this approach is exact in the harmonic limit, provided we can neglect nonadiabatic electronic transitions which occur as a result of the atomic displacements. As discussed in detail by Brovman and Kagan,[50] such processes can be neglected with reasonable confidence.

The equations of motion of the nuclei and of the electron degrees of freedom are, respectively, given by

$$M\ddot{u}_\alpha(l)=-\sum_{l'\beta}\Phi_{\alpha\beta}(ll')u_\beta(l')$$
$$-\sum_{\Gamma}\sum_{l'jk}\Phi_{\alpha k}(\Gamma;l,l'j)\Delta c_{\Gamma k}(l'j) , \tag{9}$$

$$m_\Gamma\Delta\ddot{c}_{\Gamma k}(lj)=-\sum_{l'\alpha}\Phi_{k\alpha}(\Gamma;lj,l')u_\alpha(l')$$
$$-\sum_{\Gamma'}\sum_{l'j'k'}\Phi_{kk'}(\Gamma\Gamma';lj,l'j')$$
$$\times\Delta c_{\Gamma' k'}(l'j') , \tag{10}$$

where M is the ionic mass and m_Γ denotes the effective mass of the electron pseudocharge. In the adiabatic approximation used here, the electronic mass is set equal to zero. Physically, this means that the electrons have no inertia and can instantaneously follow the motion of the ion cores.

Next, the equations of motion are Fourier transformed, resulting in new coupling terms:

$$R_{\alpha\beta}(\mathbf{q})=\sum_{l'}\Phi_{\alpha\beta}(ll')e^{i\mathbf{q}[\mathbf{r}(l')-\mathbf{r}(l)]}\ , \tag{11a}$$

$$T_{\alpha k}(\Gamma j;\mathbf{q})=\sum_{l'}\Phi_{\alpha k}(\Gamma;l,l'j)e^{i\mathbf{q}[\mathbf{r}(l'j)-\mathbf{r}(l)]}\ , \tag{11b}$$

$$H_{kk'}(\Gamma j\Gamma' j';\mathbf{q})=\sum_{l'}\Phi_{kk'}(\Gamma\Gamma';ljl'j')e^{i\mathbf{q}\cdot[\mathbf{r}(l'j')-\mathbf{r}(lj)]}\ , \tag{11c}$$

with the adiabatic condition $m_\Gamma=0$. Equation (10) allows us to eliminate $\Delta c_{\Gamma k}(lj)$ from Eq. (9). Thus, the equation of motion can be reduced to the following equation for the ionic displacement vectors $\mathbf{u}(\mathbf{q},i)$ and their associated frequencies $\omega(\mathbf{q},i)$:

$$M\omega^2(\mathbf{q},i)\mathbf{u}(\mathbf{q},i)=(R-TH^{-1}T^{\dagger})\mathbf{u}(\mathbf{q},i)\ . \tag{12}$$

Diagonalization of the dynamical matrix in Eq. (12) provides the frequencies and the polarization vectors of the phonon modes of the solid.

The multipolar oscillations of the electronic pseudocharges resulting from the ionic displacements can also be calculated in an analogous fashion from Eq. (10):

$$\Delta c_{\Gamma k}(\mathbf{q},i)=-H^{-1}T^{\dagger}\mathbf{u}(\mathbf{q},i). \tag{13}$$

The generalized force-constant matrices R, T, and H are subject to the usual constraints which follow from the invariance of the total energy with respect to infinitesimal rigid-body translations and rotations.[51]

IV. CALCULATION OF BULK-PHONON-DISPERSION CURVES

The integrals in Eqs. (8) containing the functional derivatives of the total energy with respect to $n(\mathbf{r})$, are quantities which may in principle be obtained from *ab initio* density-functional calculations. In the phenomenological approach adopted here, they are treated as fitting parameters. By an appropriate choice of the special points, both an accurate mapping of the electron density as well as its dynamical behavior are achieved with a small number of independent multipole components.

In this work we have chosen the midpoints between nearest-neighbor ions as expansion centers (point group in the bulk: D_{2h}). There are six pseudocharges per unit cell. Those surrounding the ion at the origin have the positions

$$R_1=(\tfrac{1}{2},-\tfrac{1}{2},0)a,\quad R_2=(\tfrac{1}{2},0,\tfrac{1}{2})a,\quad R_3=(0,\tfrac{1}{2},-\tfrac{1}{2})a\ ,$$
$$R_4=(\tfrac{1}{2},\tfrac{1}{2},0)a,\quad R_5=(\tfrac{1}{2},0,-\tfrac{1}{2})a,\quad R_6=(0,\tfrac{1}{2},\tfrac{1}{2})a\ , \tag{14}$$

where $a=1.805$ Å is half of the cubic cell edge in bulk copper. The resulting fcc unit cell with four atoms with the location of the 24 electronic pseudocharges is shown in Fig. 6. In Fig. 6(a) we see that the pseudocharges are in planes normal to the three Cartesian axes. They form simple square lattices in planes containing the ion cores and face-centered square structures in the planes midway between the lattice planes. Figure 6(b) shows the local

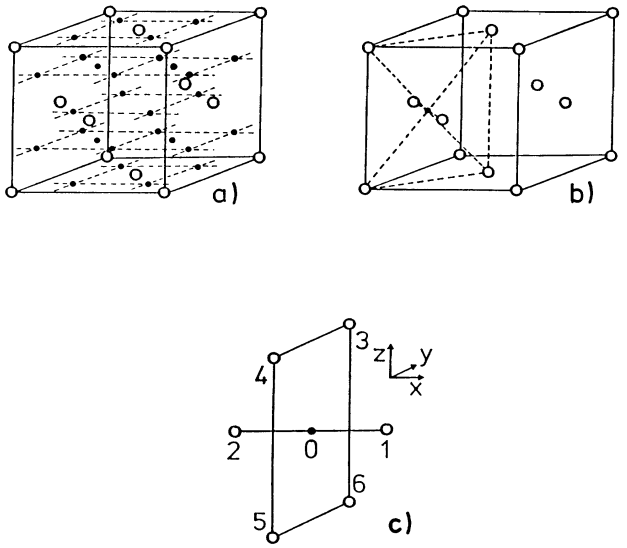

FIG. 6. (a) Schematic diagram showing the unit cell of a fcc crystal with the locations of the pseudocharges (solid circles). The unit cell contains four ion cores and 24 electronic pseudocharges. (b) The local lattice of ion cores surrounding one of the pseudocharges. (c) The first-nearest- and second-nearest-neighbor ion cores of a single pseudocharge are shown and labeled by 1 and 2 and 3, 4, 5, and 6, respectively.

geometry of the ion cores surrounding one of the pseudocharges in the dynamical model used here. The "cluster" of ions is shown separately in Fig. 6(c) and indicates the numbering of the six atoms surrounding the pseudocharge. It consists of two nearest-neighbor (NN) nuclei labeled 1 and 2 at a distance of $a/(2\sqrt{2})$ and four next-nearest nuclei (NNN) labeled 3, 4, 5, and 6 at a distance of $(a/2)\sqrt{3/2}$. This cluster belongs to the point group D_{2h}, whose eight irreducible representations Γ_i ($i=1,2,\ldots,8$) are all one dimensional.[49] The atomic displacements of the cluster and the associated distortions of the pseudocharge located at its center are projected onto a set of symmetry coordinates which transform according to the irreducible representations Γ_i. Γ_1, Γ_7, and Γ_8 are contained three times (once for radial and twice for shear displacements); Γ_2, Γ_3, Γ_4, and Γ_6 are contained twice (Γ_4 and Γ_6 have one radial coordinate; all the others are shear); and Γ_5 is contained only once (shear). The Γ_i are even for $i=1$ to 5 and odd for $i=6$ to 8. The electronic degrees of freedom of each pseudocharge, which are here considered as the most important and included in the model, are (i) one dipolar component (rigid displacement) polarized along the NN bond; this pseudocharge motion is coupled to the radial in-phase displacement Γ_6 of the NN atoms (Fig. 7, bottom left) through a coupling term B; (ii) two dipolar components (rigid displacements) polarized normal to the NN bond; these pseudocharge motions are coupled to the radial antisymmetric displacements Γ_7 and Γ_8 of the NN atoms (Fig. 7, bottom center and right) through the same coupling term H; and (iii) one single quadrupolar component,

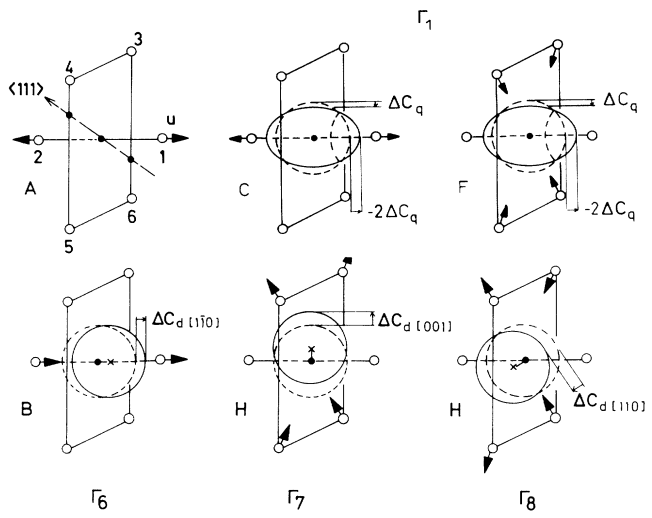

FIG. 7. Symmetry displacement patterns of the nearest-neighbor (1,2) and second-nearest-neighbor (3–6) Cu ions which couple to the pseudocharge dipolar (bottom) and quadrupolar polarizations (top, center, and right) with the corresponding irreducible representations Γ_j (point group D_{2h}) and coupling terms (B and H for dipolar polarization; C and F for quadrupolar polarization). Nearest-neighbor atoms are directly coupled by the force constant A.

transforming a sphere into a rotation ellipsoid with the axis along the NN bond; such a pseudocharge deformation, which is volume conserving and keeps the center of mass at rest, is coupled to the symmetric radial displacement Γ_1 of both NN and NNN atoms (Fig. 7, top center and right) through the coupling terms C and F, respectively.

Furthermore, the NN atoms are directly coupled through the radial force constant A (Fig. 7, top left). The coupling of the quadrupolar component transforming a sphere into a triaxial ellipsoid to the radial symmetric displacements Γ_2 of the NNN atoms is here neglected, as well as the coupling to all shear displacements. Thus, we include altogether only five effective force constants. The motions associated with the different couplings terms are described in Table II.

TABLE II. Motions and displacements associated with the force constants used in the present lattice-dynamical model.

A:	The radial nearest-neighbor (NN) Cu-Cu force constant
B:	The term coupling the Γ_6 dipolar polarization to in-phase radial displacements of the two first NN Cu ions
C:	The term coupling the Γ_1 quadrupolar polarized antiphase radial displacements of the two first NN Cu ions
H:	The term coupling the $\Gamma_{7,8}$ dipolar polarizations to in-phase radial displacements of the four second NN Cu ions
F:	The term coupling the Γ_1 quadrupolar polarized antiphase radial displacements of the four second NN Cu ions

Although the present model neglects any direct interactions between different pseudocharges, the diagonal elements of the pseudocharge-pseudocharge matrix $H_{kk}(\Gamma j,\Gamma j;\mathbf{q})$ are in general nonvanishing as a consequence of the invariance conditions. The detailed derivation of all of the matrix elements can be found in Kaden.[51]

The above coupling terms are related to the elastic constants by[51]

$$4aC_{11}=4A+2B+12H-(2C^2+18F^2-4CF)/(B+2H)$$
$$\equiv 4A_{\text{eff}}\ , \qquad (15)$$

$$4aC_{12}=2A+B+6H-(C^2+9F^2-10CF)/(B+2H)\ , \qquad (16)$$

$$4aC_{44}=2A+B+6H-(C^2+F^2+2CF)/(B+2H)\ . \qquad (17)$$

By analogy with the nearest-neighbor force-constant model, Eq. (15) is used to define the effective nearest-neighbor force constant A_{eff}. The experimental values for the elastic constant of copper[52] are

$$C_{11}(\text{exp})=1.68\times 10^{11}\ \text{N/m}^2\ ,$$
$$C_{12}(\text{exp})=1.21\times 10^{11}\ \text{N/m}^2\ , \qquad (18)$$
$$C_{44}(\text{exp})=0.75\times 10^{11}\ \text{N/m}^2\ .$$

The large derivation from the Cauchy relation ($C_{12}=C_{44}$) is generally attributed to electron-mediated many-body forces. The best fit of the Cu bulk-phonon-dispersion curves which can be obtained with one single parameter, the Cu-Cu first-nearest-neighbor radial force constant $A=28$ N/m is shown in Fig. 8(a). This best fit yields the elastic constants

$$C_{11}=A/a=1.55\times 10^{11}\ \text{N/m}^2$$

and

$$C_{12}=C_{44}=A/2a=0.77\times 10^{11}\ \text{N/m}^2$$

and, of course, cannot account for the large breakdown in the Cauchy relation.

Although the fit of the dispersion curves might be regarded as satisfactory, the only way to reproduce the correct elastic constants is to include the additional dipolar (B,H) and quadrupolar (C,F) coupling terms. It can be simply shown that the Cauchy difference implies at least a nonvanishing of F since

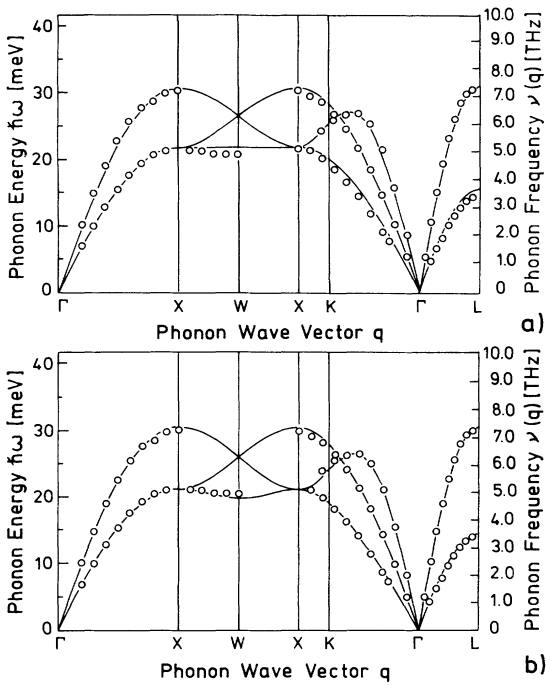

FIG. 8. The comparison of experimental neutron data (open circles) (Ref. 53) for bulk-dispersion curves of copper with those calculated from (a) the one-force-constant model with $A=28.0$ N/m and from (b) the multipole model. The multipole model provides a better fit which can be seen, for example, in the lowest T branch between X and W and Γ and L.

$$C_{12}-C_{44}=2F(3C-2F)/(B+2H)a \ . \tag{19}$$

The best fit of the bulk neutron dispersion curves[53] shown in Fig. 8(b), as obtained by minimizing χ^2, leads to the coupling parameters in Table III. As shown in Fig. 8(b), the overall agreement with the neutron data is very good and the average deviation is 1.4%. The corresponding elastic constants are

$$\begin{aligned} C_{11}(\text{fit})&=1.68\times10^{11}\ \text{N/m}^2\ (1.68)\ , \\ C_{12}(\text{fit})&=1.18\times10^{11}\ \text{N/m}^2\ (1.21)\ , \\ C_{44}(\text{fit})&=0.77\times10^{11}\ \text{N/m}^2\ (0.75)\ , \end{aligned} \tag{20}$$

where the values in parentheses are the experimental values. The average deviation of the elastic constants from the experimental values is about 5%. The Cauchy difference is 0.40×10^{11} N/m^2 and 13% smaller than the experimental value of 0.46×10^{11} N/m^2.

TABLE III. Coupling terms (all values in N/m) obtained with the present model from a best fit of bulk- and surface-phonon-dispersion curves and bulk elastic constants.

	Bulk coupling term	Surface coupling term
A	28.6	28.6
B	1.1	1.1
C	7.8	11.0
H	2.5	0.9
F	2.4	2.4

V. CALCULATION OF SURFACE-PHONON-DISPERSION CURVES

The surface-phonon-dispersion curves and the surface projected phonon densities have been calculated for the (111) surface using a slab of 33 atomic layers. As shown in Fig. 9, in the (111) direction the atomic layers contain three pseudocharges per unit surface cell and are intercalated by layers containing only pseudocharges, also three per unit cell. Thus, one of the two slab surfaces terminates with a pseudocharge layer, and symmetry requires that its charge is equally redistributed between the two slab surfaces. Thus, $\frac{3}{2}$ pseudocharges per unit cell in addition to the three already in the surface layer have to be accounted for. Assuming one conduction electron per ion core, $\frac{1}{6}$ of an electron is available per pseudocharge and $\frac{1}{4}$ of an electron has to be accommodated in the surface layer or slightly below. This corresponds to adding 0.25 electrons to each surface ion. This agrees nicely with the calculations of Euceda *et al.*[37] for Cu(111) which predict that there are in the bulk 1.115 *sp* electrons per atom, whereas at the surface there are 1.346 *sp* electrons per atom, i.e., an increase of 0.231 more electrons per atom. The dynamical effect of such an increase in charge is accounted for in the model by changing the dipolar and quadrupolar deformabilities at the surface. In this calculation the unit cell has $33\times24-12=780$ electronic degrees of freedom, which gives a 879×879 dynamical matrix for the slab. Adiabatic conditions yield a 99×99 effective dynamical matrix which has to be diagonalized.

The additional charge at the surface is expected to affect both the dipolar and quadrupolar coupling terms linking the surface pseudocharges to the ion cores. In order to fit the experimental surface-phonon-dispersion

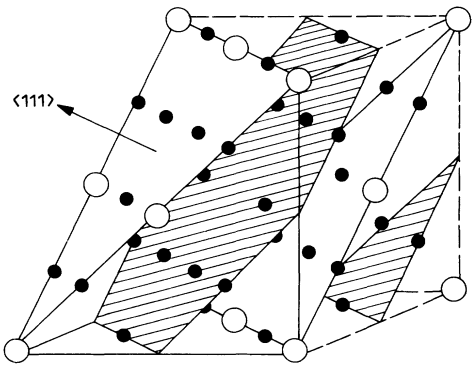

FIG. 9. Schematic diagram showing the atoms (dashed circles) and the pseudocharge locations (solid circles) used in the multipole expansion for a set of (111) planes of a fcc crystal. The atoms are located in each second plane only, whereas the pseudocharges form the same triangle-honeycomb lattice in all planes.

curves and reproduce the softening of the anomalous longitudinal resonance and the gap mode frequency at $\bar{M}$ measured by EELS,[10] we need a softening of the second-neighbor dipolar coupling term H by $\Delta H=-1.6$ N/m and a more substantial increase of the nearest-neighbor quadrupolar coupling term C by $\Delta C=3.2$ N/m. The best-fit calculated surface-phonon-dispersion curves along both symmetry directions with the parameters in the second column of Table III are compared with all the available He scattering and EELS data in Fig. 10. The quality of the fit is comparable to the best fit obtained using a total of 14 force constants in a Born–von Kármán scheme.[54]

The relative change of the effective nearest-neighbor force constant is approximately given by differentiating Eq. (15):

$$\frac{\Delta A_{\text{eff}}}{A_{\text{eff}}}=3\left[1+\frac{C^2+9F^2-2CF}{(B+2H)^2}\right]\frac{\Delta H}{A_{\text{eff}}}+\frac{F-C}{B+2H}\frac{\Delta C}{A_{\text{eff}}}\ . \tag{21}$$

With the values of Table III and the values for ΔH and ΔC given above, we obtain the dipolar and quadrupolar contributions to the effective nearest-neighbor force constant:

$$\frac{\Delta A_{\text{eff}}}{A_{\text{eff}}}=-0.26(\text{dipole})-0.09(\text{quadrupole})=-0.35\ .$$

The total reduction amounts to 35%, in essential agreement with Jayanthi *et al.*,[36] 26% coming from dipolar and 9% from quadrupolar contributions.

One of the attractive features of the present theory is that no assumptions about the physical size of the dipolar and quadrupolar polarizabilities are required. The actual electronic distortions Δc_Γ do not enter in explicitly since their effect is projected onto the ion-core displacements

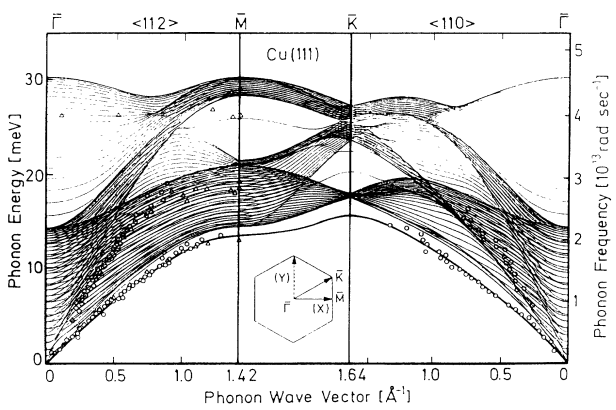

FIG. 10. Comparison of surface-phonon-dispersion curves of Cu(111) calculated by the pseudocharge multipole model along the two symmetry directions with the experimental He-scattering data (open squares) and the EELS data (open triangles) which is available only for the $\bar{\Gamma}$-$\bar{M}$ direction.

TABLE IV. Comparison of the pseudocharge dipole and quadrupole polarizabilities in the bulk and at the surface of Cu(111).

	Bulk	Surface
Dipole polarizability α_d (cm^3)	2.26×10^{-24}	6.04×10^{-24}
Quadrupole polarizability α_q (cm^5)	2.1×10^{-40}	2.9×10^{-40}

via Eq. (13). For a better physical understanding, we now estimate the actual physical size of the pseudocharges. First, we note that the above force-constant adjustments and the change in surface charge will jointly contribute to an enhancement of the dipolar and quadrupolar polarizabilities of the pseudocharges, α_d and α_q, respectively. The isotropic component of the bulk dipolar polarizability is given by an average over the inverse of the dipolar force constants[55]

$$\alpha_d^b=\frac{z_b^2}{3}\left[\frac{1}{2B}+\frac{1}{H}\right]=2.26\times10^{-24}\ \text{cm}^3\ , \tag{22}$$

where $z_b=\frac{1}{6}\times1.115e$ is the pseudocharge in the bulk if we use the charge distribution calculated by Euceda, Bylander, and Kleinman.[37] At the surface the isotropic component of the dipole polarizability becomes

$$\alpha_d^s=\frac{z_s^2}{3}\left[\frac{1}{2B}+\frac{1}{H+\Delta H}\right]=6.04\times10^{-24}\ \text{cm}^3\ , \tag{23}$$

where ΔH is given above. The value of α_d^s as given in Eq. (23) was obtained with $z_s=\frac{1}{6}\times1.346e$ from the work of Euceda, Bylander, and Kleinman.[37] Similarly, the coupling term C has an empirical link to the quadrupolar polarizability. For an assumed isotropic quadrupole polarizability, the bulk value is proportional to the average over the inverse quadrupolar coupling terms:

$$\alpha_q^b\simeq\frac{z_b^2}{12}a^2\left[\frac{1}{C}+\frac{2}{F}\right]=2.1\times10^{-40}\ \text{cm}^5\ . \tag{24}$$

The surface quadrupole polarizability is then calculated to be

$$\alpha_q^s\simeq\frac{z_s^2}{12}a^2\left[\frac{1}{C+\Delta C}+\frac{2}{F}\right]=2.9\times10^{-40}\ \text{cm}^5\ , \tag{25}$$

where the increase in charge z_s more than outweighs the increase in the force constant C. As summarized in Table IV, α_d is increased by 125% and α_q by 38% at the surface compared to the bulk.

VI. SURFACE DENSITY OF STATES

The contribution of the pseudocharge motion to the dynamic corrugation of the surface is surprisingly large compared to that of the atomic motion. In Fig. 11 we compare the surface-phonon densities of states of the ion-core motions (top) with those of the pseudocharge

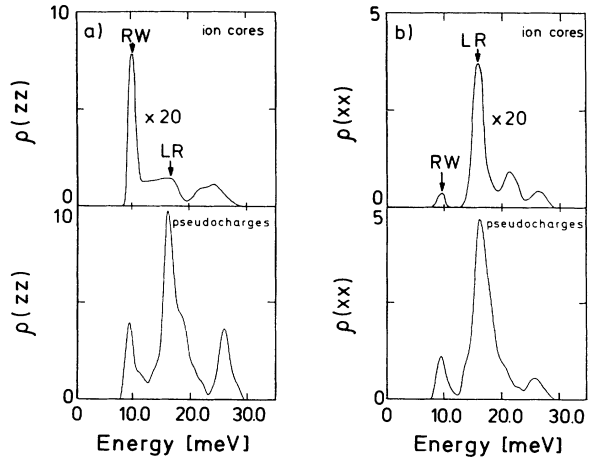

FIG. 11. Calculated phonon density of states for $\bar{M}/2$ for (a) the shear-vertical and (b) the longitudinal displacements of the ion-core motions (top) and pseudocharge motions (bottom) of the first layer. The pseudocharge calculation contains both the dipole and the quadrupole contributions with the same weight.

motions (bottom) of the first surface layer for Q at one half of the zone in the $\bar{\Gamma}\bar{M}$ direction. The DOS's are calculated according to Eq. (1), but in the case of the pseudocharge, the multipolar oscillations are used in the equation instead of the ionic displacement components. On the left side, we show the surface DOS for shear-vertical displacements normal to the surface, and on the right side, the DOS component for longitudinal displacements. In Fig. 12 we plot the same surface DOS components for Q at the $\bar{M}$ point. For simplicity the contributions of the dipolar and quadrupolar deformations to the pseudocharge components have been given the same weight. It is interesting to note a good qualitative agreement between the ion-core density of states in Figs. 11 and 12 with that calculated with the single force-constant model of Mohammed *et al.*[10] in Fig. 5. The most salient

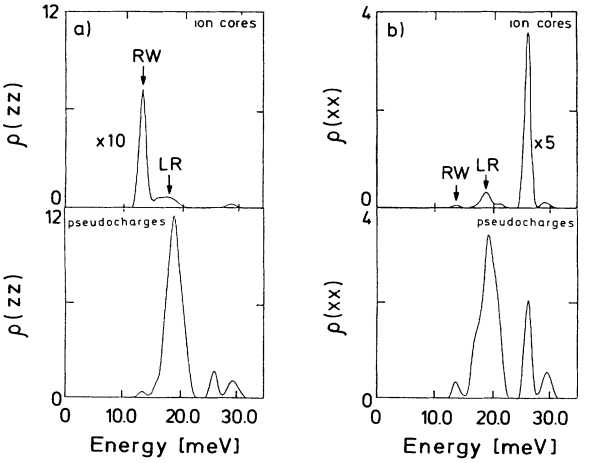

FIG. 12. Same as Fig. 11 for the $\bar{M}$ point.

feature in Figs. 11 and 12 is that at both values of Q, there is a large contribution of the pseudocharges to the longitudinal resonance in the shear-vertical normal direction. This provides by itself a mechanism for the intense He-atom scattering from the longitudinal resonance. This, however, is more directly demonstrated by a detailed calculation of the inelastic-scattering cross section, which is discussed in Sec. VII.

VII. CALCULATION OF INTENSITIES FOR COMPARISON WITH HAS-TOF SPECTRA

In the present pseudocharge multipolar scheme, an additional coupling to the phonons is provided by the modulation of the density of the electrons induced by the atomic vibrations at distances of about 3 Å above the first layer where the impulsive interaction of the helium atoms takes place. At the surface the partitioning of the electronic density given by Eq. (4) has to obey the requirement that the total electron density including that of the ion cores is nearly perfectly smooth along the surface, as indicated by the very weak He diffraction intensities on the low index surfaces.[56] This is shown schematically in Fig. 13(a) where in equilibrium the electronic densities associated with the ions and the pseudocharges are shown to add up to a constant value at distances of about 3 Å from the surface. Figure 13(b) illustrates how a rigid longitudinal displacement of the entire pseudocharge, corresponding to a dipolar deformation, yields a corrugation

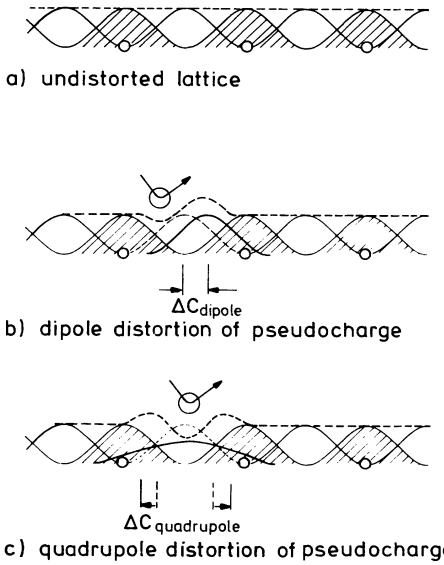

FIG. 13. (a) Schematic diagram showing the electron density distribution due to the ion cores (dashed areas) and the pseudocharges (open areas). (b) The same surface is shown but with a lateral shift of a pseudocharge corresponding to a dipole distortion as a result of the interaction with an incident helium atom. (c) The same surface is shown but with a broadening of the pseudocharge distribution corresponding to a quadrupole distribution as a result of the interaction with an incident helium atom.

of the surface charge density. A quadrupolar volume-conserving deformation of the pseudocharge leads to a more complex corrugation of the surface electron density profile as shown in Fig. 13(c). A similar corrugation and partitioning are also expected to hold for the scattering potential if it is assumed that the potential is directly related to the electron density as for example in the Nørskov relationship[38] or any other linear relationship:

$$V(\mathbf{r})=\int k(\mathbf{r},\mathbf{r}')n(\mathbf{r}')d\mathbf{r}' , \tag{26}$$

linking the scattering potential $V(\mathbf{r})$ of a He atom at $\mathbf{r}$ to the electron density $n(\mathbf{r})$, where $k(\mathbf{r},\mathbf{r}')$ is some function.

From Eqs. (4) and (5) we have

$$V(\mathbf{r})=\sum_{lj\Gamma k} c_{\Gamma k}(lj)\int k(\mathbf{r},\mathbf{r}')Y_{\Gamma k}(\mathbf{r}'-\mathbf{R}_{lj})d\mathbf{r}' , \tag{27}$$

where R_{lj} represent either the equilibrium surface atomic positions for the tightly bound core electrons (d-like; $j=0$) or the equilibrium pseudocharge positions for the conduction electrons (sp; $j=1,2,3$). The potential oscillations due to the surface vibrations are then given by

$$\Delta V(\mathbf{r})=\sum_{lj\Gamma k} F_{lj\Gamma k}(\mathbf{r})\Delta c_{\Gamma k}(lj) , \tag{28}$$

where

$$F_{lj\Gamma k}(\mathbf{r})=\int k(\mathbf{r},\mathbf{r}')Y_{\Gamma k}(\mathbf{r}'-\mathbf{R}_{lj})d\mathbf{r}' \tag{29}$$

are generalized force components describing the He atom-phonon coupling.

The inelastic-scattering probability will be proportional to the square modulus of the matrix element of the two-dimensional Fourier transform of $\Delta V(\mathbf{r})$ between initial and final states of the He atom. This matrix element is expressed by

$$\langle\chi_{iz}|\Delta V(\mathbf{Q},z)|\chi_{fz}\rangle = \sum_{j\Gamma k}\left[\int\frac{d\mathbf{R}}{4\pi^2}e^{i\mathbf{Q}\cdot(\mathbf{R}-\mathbf{R}_j)}\langle\chi_{iz}|F_{j\Gamma k}(\mathbf{r})|\chi_{fz}\rangle\right] \times\Delta c_{\Gamma k}(\mathbf{Q},j)\equiv f_a+f_d+f_q , \tag{30}$$

where $\mathbf{Q}$ is the phonon wave vector, and χ_{iz} and χ_{fz} are the wave functions for the He-atom motions normal to the surface in the initial and final states, respectively. We have set $\mathbf{r}=(\mathbf{R},z)$, $\mathbf{R}$ being the two-dimensional projection of $\mathbf{r}$ on the surface plane. The vectors $\mathbf{R}_j$, F, and Δc refer now to any arbitrary cell l, say, $l=0$, and the index l has been dropped for simplicity. The cell origin is taken at the ion site $\mathbf{R}_0=0$.

In the present dynamical model only the pseudocharges are polarizable, whereas the bound electrons are assumed to follow rigidly the motion of their respective ion cores, their polarizabilities being neglected. Thus the bound-electron dipole displacements are identical to the respective ion displacements

$$\Delta c_{\text{dipole},\alpha}(\mathbf{Q},0)\equiv u_\alpha(Q) .$$

The matrix element Eq. (30) is therefore a sum of three terms, one of which is proportional to the atomic displacement u_α; the second term is proportional to the pseudocharge dipole deformation $\Delta c_{d,d}(j)$; and the third term is proportional to the pseudocharge quadrupole deformation $\Delta c_{q,3\alpha^2-\rho^2}(j)$, where α is the component of $\boldsymbol{\rho}\equiv\mathbf{r}-\mathbf{R}_j$ on the axis of the jth pseudocharge. Note that there are three contributions from the three pseudocharges ($j=1-3$) to each of the two pseudocharge terms in the unit cell, weighted by the respective phase factors $e^{i\mathbf{Q}\cdot\mathbf{R}_j}$.

Consistent with the Born-Mayer exponential form $v(\rho)=v_0\exp(-\beta\rho)$ chosen by Bortolani *et al.* for the He-surface atom potential,[7] we set

$$F_{jd,\gamma}(\mathbf{r})=v_0\beta e^{-\beta\rho}\rho_\gamma/\rho,\ j=0,1,2,3 , \tag{31}$$

$$F_{jq,3\alpha^2-\rho^2}=v_0\beta e^{-\beta\rho}\left[3\frac{\alpha^2}{\rho^2}-1\right],\quad j=1,2,3 \tag{32}$$

with $\beta=2.2$ Å^{-1}.[7]

For lack of any *a priori* information on the He-atom pseudocharge potential, we have had to rather arbitrarily assume that the repulsive parameter β is the same for the electronic charge density surrounding the ions, which is mainly of d origin, and that of the pseudocharges, which is mainly of sp origin. Since the He interaction potential for these surfaces, however, shows very little corrugation,[56] it seems quite reasonable to assume the same repulsive force parameters for the pseudocharges between the atoms and at the ion-core positions.

Integration of Eq. (30) gives

$$f_a=v'_{if}(\beta u_z+iQu_x) , \tag{33}$$

$$f_d=\tfrac{1}{3}v'_{if}\sum_j[\beta\Delta c_{dz}(j)+iQ\Delta c_{dx}(j)]e^{-i\mathbf{Q}\cdot\mathbf{R}_j} , \tag{34}$$

$$f_q=\tfrac{1}{3}v'_{if}\sum_j\beta\Delta c_{q,3\alpha^2-\rho^2}(j)e^{-i\mathbf{Q}\cdot\mathbf{R}_j} , \tag{35}$$

with

$$v'_{if}=-\left\langle\chi_{iz}\left|\frac{\partial v}{\partial z}\right|\chi_{fz}\right\rangle .$$

The components of the pseudovector $\Delta c_{\Gamma k}(j)$ are in turn related to the ion displacement vectors through Eq. (13).

In the framework of the distorted-wave Born approximation, we have calculated the inelastic one-phonon scattering cross section per unit area for an incident atom with initial momentum $(\mathbf{K}_j,k_{iz})$ and energy E_i, and final momentum $(\mathbf{K}_f,k_{fz})$ and energy E_f. The expression first derived by Bortolani *et al.*[7,18] is easily modified by including Eqs. (34) and (35) for the forces on the pseudocharges:

$$\frac{d^2R}{dE_f d\Omega_f}=\sum_{\mathbf{Q},j}|f_a+f_d+f_q|^2\frac{(2mE_f)^{1/2}}{\omega(\mathbf{Q},j)|k_{iz}||k_{fz}|} \times\exp(-Q^2/Q_c^2)n[\omega(\mathbf{Q},j)]\delta(\mathbf{K}_f-\mathbf{K}_i-\mathbf{Q}) \times\delta(E_f-E_i-\hbar\omega(\mathbf{Q},j)) . \tag{36}$$

Here, m is the mass of the helium atom; Q_c is the cutoff parameter, which for Cu is 0.73 Å^{-1};[7] $n(\omega)$ is the Bose occupation number, and $\omega(\mathbf{Q},j)$ is the phonon frequency

of the jth mode with parallel wave vector $\mathbf{Q}$. Note that the force components are functions of the phonon wave vector $\mathbf{Q}$ and branch index j through the corresponding vectors $\mathbf{u}$ and Δc.

In order to gain insight into the role of the electronic density deformations in the scattering mechanism, we calculated the effective force-weighted surface-phonon density of states given by f_a / v'_{if}. The results for the ion-core motion (f_a) are compared with the total pseudocharge displacement ($f_d + f_q$) obtained for wave vectors along the $\bar{\Gamma}\bar{M}$ direction in Fig. 14. The ion-core density of states [Fig. 14(a)] reveals a large intensity of the surface-localized Rayleigh wave as well as the high-frequency gap mode S_2 which reach a maximum at the zone boundary. Although the position in the energy spectrum is in agreement with the experimental data, the longitudinal resonance exhibits a negligible intensity. The contribution from the pseudocharge dipolar and quadrupolar deformations is shown in Fig. 14(b). Here the effective density of states is characterized by a strong increase in the intensity of the longitudinal resonance starting at a phonon wave vector of about one-half the distance to the zone boundary and extending out to the zone boundary. The Rayleigh-wave density of states reaches its maximum at one-half of the Brillouin zone and then decreases to zero at the zone boundary. In connection with the EELS experiments, it is interesting to note that in the antiphase vertical motion of the first two planes, the surface pseudocharges are pushed up and pulled down by the motion of the underlying ions. This may provide the explanation for the intense and broad resonance in the high-energy part of the EELS spectrum.

Figure 15 compares the dipolar contribution of the force-weighted density of states with the quadrupolar contribution. The results in Fig. 15(a) suggest that the dipolar distortions may be essentially responsible for the high-frequency vertical resonance at about 30 meV and to a lesser extent to the gap mode S_2. Finally, in Fig. 15(b) it is seen that the purely quadrupolar deformations contribute substantially to the longitudinal resonance, with a maximum intensity at about two-thirds out to the zone boundary. The crucial role of the electronic defor-

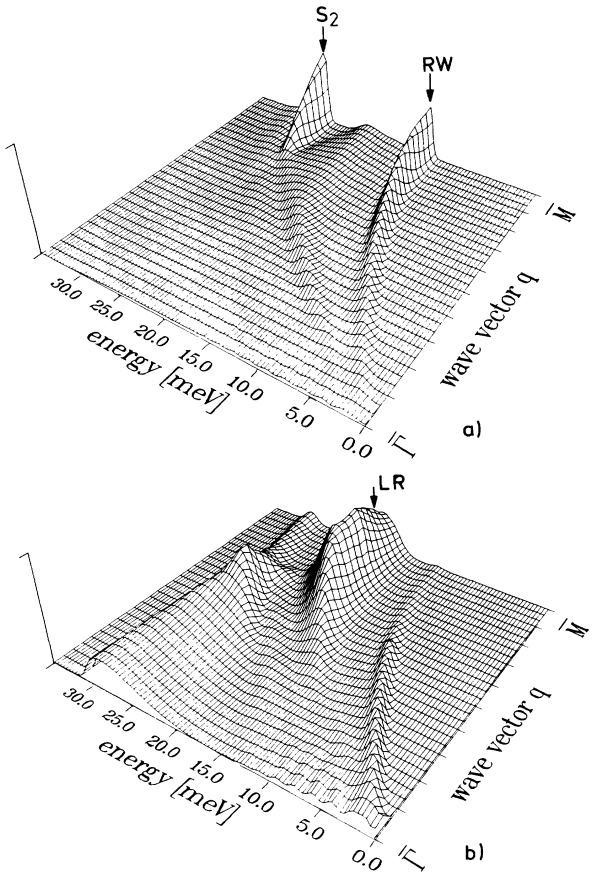

FIG. 14. Force-weighted surface-phonon density of states entering the He-scattering cross section for Cu(111) along $\bar{\Gamma}\bar{M}$: (a) shows the ion-core displacement contribution (maximum corresponds to 5.02 arbitrary units). (b) shows the pseudocharge contribution (maximum corresponding to 4.69 arbitrary units).

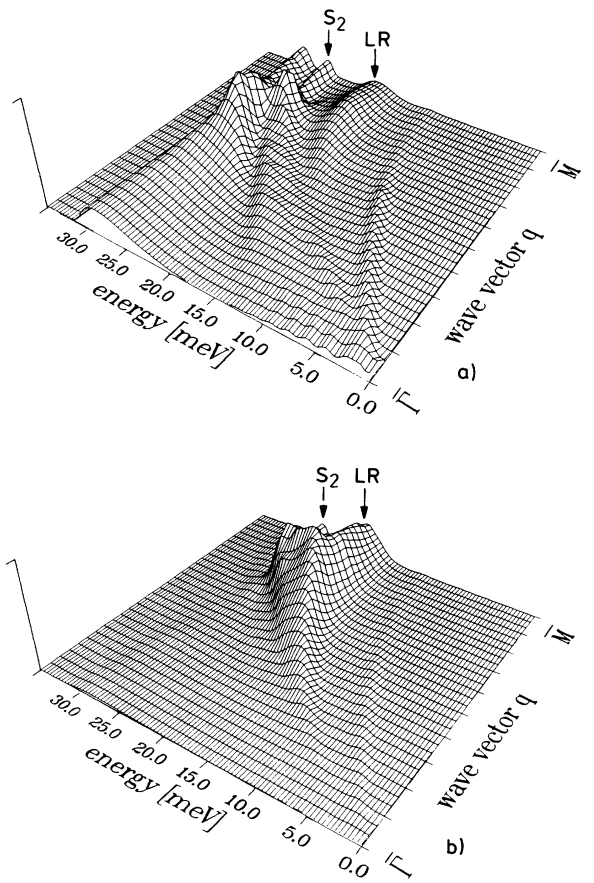

FIG. 15. Force-weighted surface-phonon density of states entering the He-scattering cross section for Cu(111) along $\bar{\Gamma}\bar{M}$: (a) shows the pseudocharge dipoloar contribution (maximum corresponds to 3.66 arbitrary units); (b) shows the pseudocharge quadrupolar contribution (maximum corresponds to 2.44 arbitrary units).

mations will be even more evident from the comparison with the calculated HAS inelastic one-phonon scattering intensities discussed next.

In Fig. 16 we compare the time-of-flight spectra calculated from Eq. (36) including first only the purely atomic contribution (dashed line) and also with the additional forces due to the pseudocharge deformations (solid line) with the He-scattering data for both symmetry directions. The dashed-line time-of-flight spectra is calculated as in the work of Bortolani *et al.* with only the interaction with the ion cores ($f_q=f_d=0$). The results indicate that only the Rayleigh wave has an appreciable intensity, whereas there is usually only a relatively small or negligible intensity associated with the longitudinal resonance. The inclusion of the pseudocharge contributions ($f_q\neq 0$, $f_d\neq 0$) increases substantially the intensities of the longitudinal mode in the time-of-flight spectra. Since the data are not calibrated in terms of absolute cross sections, the ordinates of each calculated time-of-flight spectrum with both pseudocharge and ion-core contributions were adjusted to fit the maximum of the Rayleigh peak at $\Theta_i=32°$. The relative distributions for the two theoretical curves are, of course, determined by the theory. While the peaks attributed to the Rayleigh wave near the zone boundary are practically unaffected by the additional pseudocharge contribution, the features due to the longitudinal resonance show a remarkable increase, especially near the zone boundary. At the zone boundary the antiphase shear-vertical normal motion of neighboring ions keeps the pseudocharge at rest, and the indirect forces via interactions of the He atoms with the pseudocharges are expected to be small. On the contrary, the antiphase in-plane motion of neighboring surface ions in the longitudinal mode squeezes the interposed charges inducing quadrupolar deformation, and the coupling of the He atoms to these motions is expected to be much greater. This effect is responsible for the large intensity at the longitudinal resonance, particularly at large wave vectors.

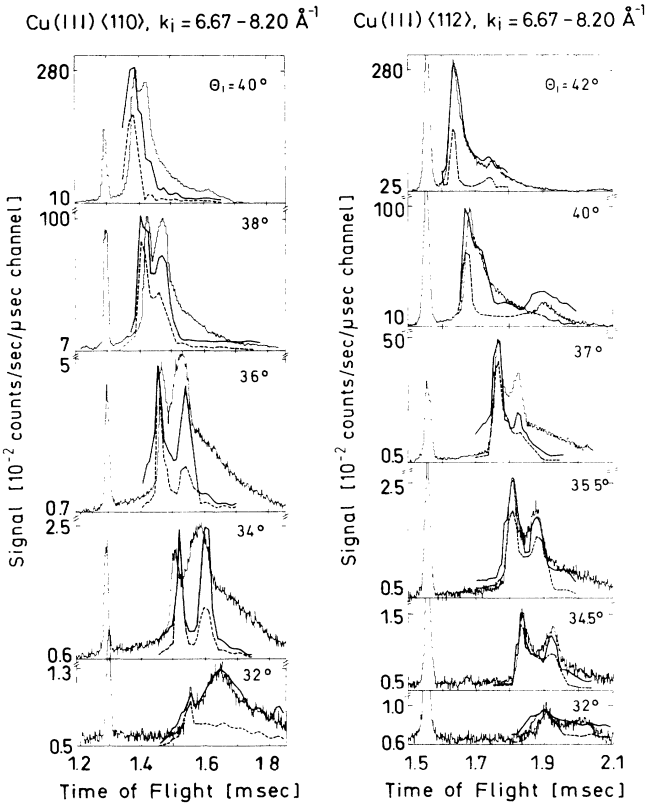

FIG. 16. Comparison of simulated time-of-flight spectra for two models with the measured time-of-flight spectra (histograms). The calculation based only on ion-core interaction (dashed-line curve) and those with dipolar and quadrupolar coupling have been normalized at the Rayleigh peak at $\Theta_i=32°$. In (a) the experimental spectra and the conditions are the same as those shown in Fig. 1 and in (b) they are the same as those of Fig. 2.

A comparison of the two calculations of the longitudinal-mode intensities indicates that the pseudocharge contributions are considerable. This explains in a simple way the unexpectedly large He-scattering intensity from the longitudinal resonance. We recall that the previous explanation by Bortolani *et al.*[11] invoked an unusually strong surface force-constant perturbation in order to endow the resonance with a strong elliptical polarization, with an especially large vertical component. The present picture explains the appearance, the position, and the intensity of the longitudinal resonance, as well as of the EELS gap mode S_2 and of the high-frequency EELS active branch, only in terms of enhanced electron deformabilities in the surface region.

VIII. DISCUSSION

The present study points out in a very striking way the much greater sensitivity of surface-phonon-dispersion curves to the details of the lattice-dynamical models as compared to bulk phonons. Figure 8 showed that a single force constant could already fit the neutron data quite well. With the five-parameter pseudocharge model, a much better fit is achieved and the elastic constants are also well simulated. But for the bulk the same good description could have been obtained by the Born–von Kármán procedure simply by adding additional longer-ranged two- and three-body force constants. At the surface, however, the Bortolani-Mills paradox resulted from the extreme sensitivity of the dispersion curves and the experimental inelastic intensities to the actual force-constant model used. And, as discussed in connection with Fig. 5, in fact neither model was entirely satisfactory. Since Bortolani *et al.*[11,54] went to great efforts to optimize their fit we can, in fact, conclude that since so far no satisfactory set of Born–von Kármán force constants could be found, it appears quite likely that in fact none exists. As discussed in Sec. V, the pseudocharge model does an excellent jot not only of describing the bulk-dispersion curves but also of fitting the surface-phonon-dispersion curves in a much more satisfactory way than the force-constant models.

Whereas the pseudocharge model has been used previously for the calculation of bulk-phonon-dispersion curves[33–35] as well as surface-phonon-dispersion curves,[36]

the present paper contains the first investigation to include the inelastic interaction of gas atoms with the electronic pseudocharges at the surfaces. As a result of this coupling, in addition to that included previously through the ion cores, we find significant differences between the relative inelastic phonon intensities for the Rayleigh wave and the longitudinal resonance in He-atom and electron inelastic scattering. Since the coupling to the pseudocharges is not expected to affect the EELS intensities, because of their low-electron density, the only test of the new model is provided by the HAS intensity calculations presented in Fig. 16. There we saw that the inclusion of the inelastic interaction with the pseudocharges could indeed explain nearly quantitatively the large intensity of the longitudinal peaks.

At the same time as this theoretical study of surface phonons was going on, a series of HAS experiments on Cu(001) were carried out in our laboratory.[57] This system had already been investigated previously by EELS by two groups.[58–60] For both symmetry directions only evidence for a Rayleigh mode was found, and the results from the two different groups were in good agreement. Thus it was most surprising to find that the HAS time-of-flight spectra showed a strong longitudinal resonance in both the ⟨100⟩ and ⟨110⟩ directions.[61] In the ⟨100⟩ direction the longitudinal peak was up to *five times more intense* than the Rayleigh peak. The dispersion curve for the Rayleigh mode was in excellent agreement with the EELS data. The intensity ratio was less dramatic in the ⟨110⟩ direction where the intensity of the longitudinal mode was always less than the Rayleigh mode. This experiment thus suggests that indeed effects similar to those discussed here can be very important.[62] Calculations using the same theory presented here are presently under way for this surface.[63]

Of course, it would be highly desirable to have a more rigorous theory to describe the coupling of a He atom to the pseudocharges and the surface lattice dynamics. Unfortunately, most of the calculations of He metal surface interaction treat the surface as unstructured as in the jellium calculations of Lang[64,65] and others. It is interesting to note that these calculations do show a substantial charge redistribution in the solid directly opposite to the interacting rare-gas atom similar to that shown in Figs. 13(b) and 13(c). More detailed calculations in which an explicit account of the cores is included are not known to us.

It should be pointed out, however, that for the analogous problem of vibrational excitation of a diatomic (H_2) by He approaching from the broadside direction, quantum-chemical calculations reveal a significant charge redistribution in the bonding region of H_2 which was shown to lead to an *attraction* of the H atoms in the molecule at relatively large distances of approach of the He atom.[66] This was attributed to an increased electronic charge buildup between the protons which, via the Hellmann-Feynman theorem, leads to an additional attraction. This coupling thus leads to a mechanism for vibrational excitation of the molecule in addition to the direct repulsive interaction with the atoms of the molecule which dominates at smaller distance of approach. This charge redistribution interaction is the analog to the one discussed here.

As alternative description of the pseudocharge effect is to consider locally fluctuating dipole moments. As pointed out by Celli,[67] as the surface atoms move laterally to and fro, the dipole moment normal to the surface will also fluctuate in magnitude. This assumes that the free electrons will be largely decoupled from the ionic cores. This change in dipole moment will lead to a change in electron spillout into the vacuum which in turn will affect the interaction potential with the He atom.

Finally we point out that the present model of atom-surface interactions has important implications for the interpretation of HAS surface-phonon data in terms of surface force constants. Here it must be recalled that an analysis of the polarization of the different modes is a prerequisite to being able to derive unique information on surface force constants.[41] Thus the relative HAS intensities of different modes as discussed here have a direct effect on the force constants, and previous analysis must be reexamined in the light of the new mechanism discussed here. Beyond this, the new type of interaction proposed here has far-reaching consequences for our understanding of a variety of macroscopic phenomena, such as energy accommodation coefficients, in terms of the detailed elementary processes describing atom-surface interactions in which inelastic effects are important.[68]

ACKNOWLEDGMENTS

We are indebted to H. Bilz (deceased) for his encouraging interest in our early experiments and for first calling our attention to the possibility of a direct interaction of the atoms with surface pseudocharges. Two of us (G.B. and P.R.) gratefully acknowledge the support of the Alexander von Humboldt Foundation, Germany. We are grateful to Douglas Mills (University of California, Irvine) for stimulating correspondence, to Vittorio Celli (University of Virginia) for useful discussions, and to D. Himes for calculating the multiphonon background in Fig. 4. Finally we thank G. Santoro for providing us with the calculations shown in Fig. 5.

*Present address: University of Stuttgart, Pfaffenwaldring 57, 7000 Stuttgart 80, Federal Republic of Germany.

†Present address: Department of Chemistry, University of Toronto, 80 St. George Street, Toronto, Canada.

‡Permanent address: Dipartimento di Fisica, Dell'Universitá di Milano, via Celoria 16, 20133 Milano, Italy.

[1] J. P. Toennies, in *Proceedings of the Solvay Conference on Surface Science*, edited by F. de Wette (Springer-Verlag, Heidelberg, 1988), p. 248.

[2] H. Ibach, J. Vac. Sci. Technol. A **5**, 419 (1987).

[3] J. P. Toennies, J. Vac. Sci. Technol. A **5**, 440 (1987).

[4] R. B. Doak, U. Harten, and J. P. Toennies, Phys. Rev. Lett. **51**,

578 (1983).
[5]U. Harten, J. P. Toennies, and Ch. Wöll, Faraday Discuss. Chem. Soc. **80**, 137 (1985).
[6]G. Zhang (unpublished).
[7]V. Bortolani, A. Franchini, F. Nizzoli, and G. Santoro, Phys. Rev. Lett. **52**, 429 (1984).
[8]V. Bortolani, G. Santoro, U. Harten, and J. P. Toennies, Surf. Sci. **148**, 82 (1984).
[9]V. Bortolani, A. Franchini, and G. Santoro, in *Electronic Structure, Dynamics, and Quantum Structural Properties of Condensed Matter,* edited by J. T. Devreese and P. Van Camp (Plenum, New York, 1985), p. 401.
[10]M. H. Mohamed, L. L. Kesmodel, B. M. Hall, and D. L. Mills, Phys. Rev. B **37**, 2763 (1988); B. M. Hall, D. L. Mills, M. H. Mohamed, and L. L. Kesmodel, *ibid.* **38**, 5856 (1988).
[11]V. Bortolani, A. Franchini, and G. Santoro (unpublished).
[12]J. P. Toennies, Superlatt. Microstruct. **7**, 193 (1990).
[13]Several attempts have been made to resolve this dilemma. One proposal was that the He intensities are overmphasized by a multiphonon background (Refs. 14 and 15). On the basis of recent advances in our understanding of multiphonon processes, this explanation can now be ruled out with considerable confidence (Ref. 16). It has also been implied that part of the problem may have to do with the different schemes used to fit the bulk data (Ref. 10). Both approaches are based on the Born–von Kármán parametrization of lattice forces but differ in the number of force-consatnt parameters considered. Although this might provide for uncertainties in the size of the effect obtained, there is general agreement that this cannot account for the large extent in the gross differences.
[14]D. L. Mills (private communication).
[15]V. Celli (private communication).
[16]V. Celli, D. Himes, V. Bortolani, G. Santoro, J. P. Toennies, and G. Zhang, Surf. Sci. **242**, 518 (1991); V. Celli, D. Himes, P. Tran, J. P. Toennies, Ch. Wöll, and G. Zhang, Phys. Rev. Lett. **66**, 3160 (1991).
[17]V. Bortolani, A. Franchini, N. Garcia, F. Nizzoli, and G. Santoro, Phys. Rev. B **28**, 7358 (1983).
[18]A. Levi and V. Bartolani, Riv. Nuovo Cimento **9**, 1 (1986).
[19]V. Bortolani, A. Franchini, G. Santoro, J. P. Toennies, Ch. Wöll, and G. Zhang, Phys. Rev. B **40**, 3524 (1989).
[20]V. Celli, D. Eichenauer, A. Kaufhold, and J. P. Toennies, J. Chem. Phys. **83**, 2504 (1985).
[21]D. Eichenaure, U. Harten, J. P. Toennies, and V. Celli, J. Chem. Phys. **86**, 3693 (1987).
[22]R. Smoluchowski, Phys. Rev. **60**, 661 (1941).
[23]Additional evidence for the effect of electrons at surfaces on HAS comes from several recent experiments on, for example, W(001) [H.-J. Ernst, E. Hulpke, and J. P. Toennies, Europhys. Lett. **10**, 747 (1989)] and the layered compounds such as TaS_2 [G. Benedek, G. Brusdeylins, F. Hofmann, P. Ruggerone, J. P. Toennies, and R. Vollmer (unpublished)]. There the diffraction intensities are found to depend crucially on small modulations in the surface electron density, which in the above examples result from change-density waves, superimposed on the otherwise very smooth surface electron density distributions. In both cases these effects are more important than even the modulations caused by the ion cores. The experiments on TaS_2 indicate moreover that the phonon-induced modulation of the electron density provides the major coupling of the helium atoms to lattice vibrations.
[24]A. G. Eguiluz, A. A. Maradudin, and R. F. Wallis, Phys. Rev. Lett. **60**, 309 (1988).
[25]A. G. Eguiluz, J. A. Gaspar, M. Gester, A. Lock, and J. P. Toennies, Phys. Rev. Lett. **66**, 337 (1991).
[26]A. M. Lahee, J. P. Toennies, Ch. Wöll, K. P. Bohmen, and K. M. Ho, Europhys. Lett. **10**, 261 (1989).
[27]K. M. Ho and K. P. Bohnen, J. Electron Spectrosc. Relat. Phenom. **54/55**, 229 (1990).
[28]B. G. Dick, Jr. and A. W. Overhauser, Phys. Rev. **112**, 90 (1958).
[29]W. G. Kleppmann and W. Weber, Phys. Rev. B **20**, 1669 (1979).
[30]W. Weber, Phys. Rev. B **15**, 4789 (1977).
[31]W. Hanke and H. Bilz, Z. Naturforsch. Teil **26A**, 585 (1971).
[32]K. Fischer, H. Bilz, R. Haberkorn, and W. Weber, Phys. Status Solidi B **54**, 285 (1972).
[33]W. Wakabayashi, Solid State Commun. **23**, 737 (1977).
[34]P. B. Allen, Phys. Rev. B **16**, 5139 (1977).
[35]M. Li and W. A. Goddard III, Phys. Rev. B **40**, 12 155 (1989).
[36]C. S. Jayanthi, H. Bilz, W. Kress, and G. Benedek, Phys. Rev. Lett. **59**, 795 (1987).
[37]A. Euceda, D. M. Bylander, and L. Kleinman, Phys. Rev. B **28**, 528 (1983).
[38]N. Esbjerg and J. K. Nørskov, Phys. Rev. Lett. **45**, 807 (1980).
[39]J. P. Toennies, in *Surface Phonons,* edited by W. Kress and F. W. de Wette, Springer Series of Surface Sciences Vol. 21 (Springer, Berlin, 1991), p. 111.
[40]Tables of the data points can be obtained by writing to J. P. Toennies.
[41]G. Armand, Solid State Commun. **48**, 261 (1983).
[42]R. S. Leigh, B. Szigeti, and V. K. Tewary, Proc. R. Soc. London Ser. A **320**, 505 (1971); W. Cochran, Acta Crystallogr. Sec. A **27**, 556 (1971); N. J. Chesser and J. D. Axe, Phys. Rev. B **9**, 4060 (1974).
[43]Recently, for all three Al low-index surfaces this procedure has been shown to yield a set of force constants in good agreement with a first-principles calculation: A Franchini, V. Bortolani, G. Santoro, V. Celli, A. G. Eguiluz, J. A. Gaspar, M. Gester, A. Lock, and J. P. Toennies (unpublished).
[44]The simple force-constant calculations for $\beta_1^s=\beta_1^b$ and $\beta_{\|}^s=0.85\beta^b$ carried out by N. Luo in our laboratory show that the longitudinal resonance is not shifted downwards enough to agree with its position observed both by EELS and HAS, contrary to what is implied in Ref. 10.
[45]G. Santoro (private communication).
[46]R. Brako and D. M. Newns, Phys. Rev. Lett. **48**, 439 (1982).
[47]The multiphonon background was not accounted for in the calculation of Fig. 4. Its effect would be to reduce the relative differences in the Rayleigh and longitudinal peak intensities by no more than 30% and thus it does not have a significant effect.
[48]R. G. Parr and W. Yang, *Density Functional Theory of Atoms and Molecules* (Oxford University Press, New York, 1989).
[49]M. Tinkham, *Group Theory and Quantum Mechanics* (McGraw-Hill, New York, 1964).
[50]E. G. Brovman and Yu. M. Kagan, in *Dynamical Properties of Solids,* edited by G. K. Horton and A. A. Maradudin (North-Holland, Amsterdam, 1974), p. 191.
[51]C. Kaden (unpublished).
[52]N. A. Ashcroft and N. D. Mermin, *Solid State Physics* (Saunders, Philadelphia, 1976), p. 447.
[53]R. M. Nicklow, G. Gilat, H. G. Smith, L. J. Raubenheimer, and M. K. Wilkinson, Phys. Rev. **164**, 922 (1967).
[54]A. Franchini, dissertation, University of Modena, 1985/86.
[55]Recalling that the dipolar polarizability is the ratio of the induced dipole $z\Delta c_d$ (z=pseudocharge) to the electric field, and the latter is twice the dipolar force constant times $\Delta c_d/z$, we

have that

$$\alpha_d = z^2/(2\times\text{dipolar force constant}).$$

The quadrupolar polarizability is the ratio of the induced quadrupole to the electric-field gradient. Here we have to give the pseudocharge a conventional (spherical) volume, say, $\pi a^3/6$, and to uniformly distribute the charge z inside this volume. The induced quadrupole is approximately $za\delta c_q$, where δc_q represents now the physical deformation of the sphere, i.e., the displacement of the pseudocharge wall at the equator [as defined in Fig. 7 (top)]. The field gradient $\partial E_x/\partial x$, normal to the equitoral plane is approximately twice the quadrupole force constant times $2\delta c_q/za$, and, therefore,

$$\alpha_q \simeq z^2a^2/(4\times\text{quadrupola force constant}) .$$

The isotropic component of both polarizabilities is the average over the three orthogonal directions.

[56]The first-order He diffraction intensities along the $\langle 112\rangle$ azimuth relative to the specular peak are at incident energies of ≈ 30 meV (unless otherwise indicated): 1×10^{-3} for Ag(111) [G. Boato, P. Cantini, and R. Tatarek, in *Proceedings of the Seventh International Vacuum Congress and Third International Conference on Solid Surfaces, Vienna, 1977,* edited by R. Dobrozemsky, F. Rüdenauer, F. P. Viehböck, and A. Breth (Berger, Wien, 1977), Vol. 2, p. 1377; J. M. Horne, S. C. Yerkes, and D. R. Miller, Surf. Sci. **93**, 47 (1980)]; $<2\times10^{-4}$ for Cu(111) (Ref. 6); $\approx1\times10^{-3}$ for Au(111) at 17 meV [U. Harten, A. M. Lahee, J. P. Toennies, and Ch. Wöll, Phys. Rev. Lett. **54**, 2619 (1985)]; and 1×10^{-3} for Pt(111) (Ref. 18). A ratio of 1×10^{-3} corresponds to a corrugation amplitude of between 2×10^{-3} Å (Ref. 19) and 2×10^{-2} Å [Jonsson and Weare, Surf. Sci. **181**, 495 (1987)] depending on the computational method and model used to describe the atom-surface potential.

[57]J. Ellis, A. Reichmuth, and J. P. Toennies (unpublished).

[58]M. Wuttig, R. Franchy, and M. Ibach, Solid State Commun. **57**, 445 (1986).

[59]M. Wuttig, R. Frauchy, and H. Ibach, Z. Phys. B **65**, 71 (1986).

[60]L. L. Kesmodel, M. L. Xu, and S. Y. Tong, Phys. Rev. B **34**, 2010 (1986).

[61]Indirect evidence for such a mode in EELS on the Ag(100) surface has just recently been presenteed by Y. Chn, S. Y. Tong, M. Rocco, P. Moretto, U. Valbusa, K. P. Bohnen, and K. M. Ho, Surf. Sci. Lett. **250**, L389 (1991).

[62]Despite several attempts, it has not been possible to fit the longitudinal mode with a Born–von Kármán fit involving modified surface force constants: A Reichmuth (unpublished) and G. Santoro (private communication).

[63]N. Luo, P. Ruggerone, and J. P. Toennies (unpublished).

[64]N. D. Lang, Phys. Rev. Lett. **46**, 842 (1981).

[65]N. D. Lang and J. K. Nøskov, Phys. Rev. B **27**, 4612 (1983).

[66]M. Krasuss and F. M. Mies, J. Chem. Phys. **42**, 2703 (1965).

[67]V. Celli (private communication).

[68]V. Bortolani, G. P. Brivio, A. Franchini, T. B. Grimley, and G. Santoro, Chem. Phys. Lett. **170**, 1 (1990).

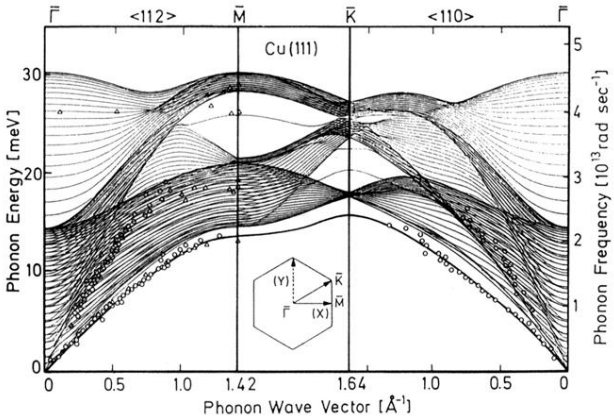

FIG. 10. Comparison of surface-phonon-dispersion curves of Cu(111) calculated by the pseudocharge multipole model along the two symmetry directions with the experimental He-scattering data (open squares) and the EELS data (open triangles) which is available only for the $\bar{\Gamma}$-$\bar{M}$ direction.